



Influence of particle size on antibacterial and antifungal strains of titanium dioxide (TiO₂) nanoparticles synthesized by SILAR method

A. A. Mohite^{ab}, A. A. Survase^{ae}, P.K.Pagare^b, H. D. Shelke^c, A. D. Kadam^d, A. S. Jadhav^e, B.S. Pawar^e and A. P. Torane^{a,b*}

^aRayat Institute of Research and Development Center, Satara - 415001(M.S.) India.

^bDepartment of Physics, Yashwantrao Chavan Institute of Science, Satara- 415001(M.S.) India.

^cAdvanced Physics Laboratory, Department of Physics, Savitribai Phule Pune University, Pune, Maharashtra 411 007, India

^dDepartment of Chemistry, Yashwantrao Chavan Institute of Science, Satara- 415001(M.S.) India.

^eDepartment of Microbiology, Yashwantrao Chavan Institute of Science, Satara- 415001(M.S.) India.

ABSTRACT:

Health and environmental toxicity are major issues. Food, medicine, textiles, food packaging, and water treatment require antimicrobial materials. Concern over the expansion of inorganic antimicrobial materials has grown due to the growing resistance of some bacteria to antibiotics and the human toxicity of several organic compounds. A various TiO₂ thin films have been prepared by SILAR method by changing dipping cycles on glass micro slides substrates at room temperature. The thickness of TiO₂ thin films is estimated to be 246, 312, 569 and 725 nm for 10, 20, 30 and 40 deposition cycles respectively. The XRD pattern has four strong peaks at $2\theta = 24.87^\circ$, 37.87° , 47.66° and 62.72° corresponding to diffraction planes of (101), (112), (200) and (204) respectively, indicates the formation of anatase (JCPDS: 00-021-1272) crystal structure of TiO₂ material. The obtained crystalline size values of (101) plane of 10, 20, 30 and 40 deposition cycles sample are 31.32, 32.94, 35.25 and 38.17 nm, respectively. It is observed that the appearance of a narrow band at 534.18 cm^{-1} may be assigned to Ti-O bond is associated the characteristic vibrational mode of anatase TiO₂. The vibrations reflected in the range between 400 and 900 cm^{-1} corresponds to TiO₂ bonds present in the deposited films. Deposition cycles of the SILAR method show significant changes in surface morphology of TiO₂ thin films. The band gap values are found to be 3.70, 3.67, 3.65 and 3.59 eV for 10, 20, 30 and 40 deposition cycles thin films, respectively. Here we observed the peaks in the region of 550 nm to 610 nm. The peaks at 576, 580 and 593 nm due to the self-trapped excitons and the oxygen vacancies in TiO₂. The antimicrobial potential of synthesized TiO₂ nanoparticles was studied using agar gel diffusion method to the zone of inhibition of two bacterial strains *S. aureus* (NCIM-2654) gram-positive, *P. aeruginosa* (NCIM-5032) gram-negative bacteria using streptomycin as positive control and distilled water as negative control. We got excellent antimicrobial activity for these samples which were prepared by 10 SILAR cycles.

Keywords: SILAR Cycle, TiO₂, Antibacterial activity

Received 22.10.2022

Revised 23.11.2022

Accepted 21.12.2022

INTRODUCTION

The potential health effects and environmental toxicity of nanoparticles (NPs) are currently important issues that need to be addressed. The persistent trend in the quest for new antimicrobial materials is due to the ubiquity of microbial occurrence in a variety of industries, including food, medicine, textiles, food packaging, and water treatment. Concern over the expansion of inorganic antimicrobial materials has grown due to the rising resistance of specific bacteria to specific antibiotics and the toxicity of several organic antimicrobial compounds to humans. Due of their all-encompassing antibacterial properties, metal and metal oxide compounds have received the most attention among these substances. In contrast, nanoscale materials stand out because of their improved characteristics, including their increased surface area to volume ratio. Antimicrobial NPs exhibit impressive and distinctive behaviours compared to their bulk characteristics [1, 2]. Numerous studies have established that metal oxide NPs, which are frequently made using chemical procedures, have revealed varying degrees of toxicity to test organisms [3-6]. The development of NPs motivated by environmental sustainability and advancements distinguished by an ecological perspective, warm reaction circumstances, and non-toxic pioneers has recently received special attention from researchers. Ecological advancements are currently being examined for the synthesis of non-toxic NPs as a result of this rising sensitivity toward green chemistry and biological processes. These methods are seen as safe, profitable, biocompatible, non-toxic, environmentally friendly,

and innately social developments [6]. Additionally, it has been established that chemically combined NPs have shown increased clustering and Decreased stability, whereas biologically generated NPs are more stable in size and require less energy to produce [7].

There is growing interest in metallic nanoparticles (NPs) that reveal antibacterial activity due to the increase of antibiotic resistance among microbial pathogens [8, 9]. Both gram-positive and gram-negative bacteria have been shown to be resistant to the antibacterial capabilities of NPs, which have also been related to NP size, optical, morphological, catalytic, photoactive, surface charge, and thermal properties [10, 11]. Furthermore, many microorganisms confirm changeable vulnerability to NPs [12, 13]. Antibiotic overuse has increased bacterial resistance to antimicrobial medications, necessitating the development of more effective antimicrobial agents to combat the resistance issue [14]. With the use of metal oxide, many materials have been created with enhanced physico-chemical components. The unique physiochemical features of metal oxide nanoparticles, such as manganese oxide (MgO), zinc oxide (ZnO), iron oxide (Fe₂O₃), and titanium dioxide (TiO₂), have made them popular in recent years for use in biological applications. TiO₂ is a well-liked semiconducting transition metal oxide material in the middle of the metal oxide antimicrobial agents, and it exhibits distinctive properties, such as simple control, low cost, non-toxicity, and noble resistance to chemical loss, that allow its application in solar cells, optics, electronics, chemical sensors, antifungal agents, and antibacterial [15]. TiO₂ nanoparticles are typically non-toxic, have excellent surface morphology, and have a large surface area. Because of their exceptional bio-related activity outside of bacterial contagion and their photocatalytic antimicrobial action, several publications have said that TiO₂ NPs are among the most carefully planned NPs [16–19]. The current study illustrates how different deposition cycles affect structural, morphological, and optical features. Additionally, synthetic TiO₂ nanoparticles were tested for their ability to inhibit the growth of three bacterial strains: *Staphylococcus aureus* (NCIM -2654), *Pseudomonas aeruginosa* (NCIM -5032), and *Candida albicans* (NCIM -3466). Possible treatments are noted.

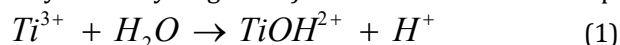
SILAR METHOD-BASED TiO₂ THIN FILM SYNTHESIS:

Material preparation:

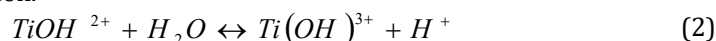
By using the SILAR process at room temperature on glass micro slide substrates, a thin coating of TiO₂ was produced. Analytical reagent (AR) grade compounds were used without additional purification. As cationic and anionic precursors, titanium (III) chloride (TiCl₃, 30 wt% in HCl, Aldrich) liquid and sodium hydroxide (NaOH, Molychem), respectively, were utilized. The doubly distilled water (DDW) used to prepare each solution. Using 30% aqueous ammonium hydroxide (NH₄OH) solution, TiCl₃ solution's pH was brought down to 3. Glass substrates were cleaned with detergent before being ultrasonically processed in DDW since the substrate is crucial to the formation of nanostructures. Glass substrate was submerged vertically in cationic precursor of 0.1 M TiCl₃ (4.8 ml) solutions in DDW for 10s in the initial phase of the synthesis of TiO₂ thin films using the SILAR method, causing a layer of titanium-water complex Ti(OH)₂²⁺ to be adsorbed on the substrate surface. The second stage involved washing the film in water for 5 seconds while the substrate was submerged in a second beaker containing DDW. In the third step, the substrate was submerged for 10 seconds in the third beaker of 0.1 M (0.4 gram) NaOH (pH = 12) solutions in DDW, where the adsorbed Ti species reacted with the NaOH to generate stable TiO₂ on the substrate. In addition to TiO₂, some unreacted titanium hydroxide was also adsorbed on the substrate. This material is washed out in the fourth step by dipping the substrate for five seconds into the fourth beaker containing DDW. As a result, one SILAR cycle is finished. To enhance the film thickness, this procedure was done in succession many times. The thickness of the TiO₂ layer varied depending on the number of deposition cycles used to coat the substrate. The substrates covered with a thin layer of TiO₂ were taken off after the recommended intervals (10 to 40 cycles), cleaned with double-distilled water, allowed to dry in the open air, and then preserved in a plastic bag. The films created using this technique were homogeneous and adhered to the substrates effectively. For two hours, these films were annealed in the air at 723 K to get rid of the hydrous content and boost crystallinity. These annealed TiO₂ substrates are employed in additional research.

Mechanisms for Film Formation and Reaction:

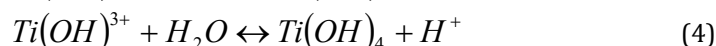
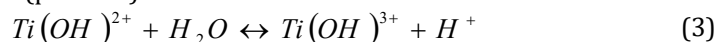
An easy and economical SILAR process was used to create the titanium dioxide (TiO₂) thin films. The following will explain how materialized the material: Because of trivalent and electrophilic nature, when TiCl₃ is dissolved in DDW, it immediately attracts the electron density from the oxygen of the water molecule, escalating (acidic hydrated hydrogen ion) in the solution and developing as per eq (1)



Aqueous ammonia increases pH to 2.5 when added to a $TiCl_3$ solution. The following reactions shed light on the impact of pH variation. Then, $Ti(OH)_2^{2+}$ species are created on the substrate, through heterogeneous reaction.



When the substrate is immersed in NaOH solution, $Ti(OH)_2^{2+}$ species quickly transition into $Ti(OH)_3^+$ species and advances to $Ti(OH)_4$ species that are dissolvable in aqueous media because of fast enrichment in OH ions (pH > 2.5).



The $Ti(OH)_4$ species are soluble in aqueous solution and remain soluble in the bath down to alkaline pH (pH > 7.0). As a result of this chemical precipitation occurs.



Finally, well-constructed particles were deposited on the surface of the substrate by nucleation and growth process after the nuclei lump by coalescence pathway. Particles stretch further to create granular nanostructures as the number of SILAR cycles increases (up to 40). The strategic advantage of SILAR is that the grain size of these particles may be altered by varying basic parameters such as temperature, dipping cycles, precursor concentration, bath pH, and time between reactions and adsorption. On glass substrates, a thin, persistent white layer was etched. Due to increasing stress on the substrate, additional cycling isolates the deposited material from the surface. All films were annealed at 723 K for 2 hours after being deposited in order to develop the crystallinity and renovate the hydroxide content.

Materials Characterization:

The BRUKER AXS D8 X-ray diffractometer ($\lambda = 1.54$) was used to examine the X-ray diffraction (XRD) patterns of the synthesized materials. A Jasco FT-IR/4100 spectrometer was used for the investigation of the Fourier transform infrared spectrum. SEM was used to examine the surface morphology of the samples (JEOL JSM-6390). The HITACHI UV4100 spectrometer was used to analyze the UV-visible optical absorption and transmission of TiO_2 thin films at room temperature in the wavelength range of 200 to 900 nm.

Microbiological activity

The sterile saline water was created with the microbiological culture's inoculums. The bacterial growth was facilitated by the nutrient agar plates. On sterile nutritional agar plates, *S. aureus* and *P. aeruginosa* cultures were distributed, and *C. albicans* fungal cultures were placed on sterile Sabouraud agar plates. Wells were made in these plates using a sterile cork borer. With the aid of a micropipette, TiO_2 nanomaterial were dissolved in sterile, distilled water, and plates were incubated at 37°C for 24 hours to assess their antibacterial activity.

RESULTS AND DISCUSSION:

Determination of thickness:

Fig. 1 depicts the variation in TiO_2 film thickness with different deposition cycles. The expansion of the nucleation and coalescence process is responsible for the nonlinear rate of rise in layer thickness with deposition cycles. Additional nucleation sites provide coagulation throughout the rising process. For 10, 20, 30, and 40 deposition cycles, the thickness of TiO_2 thin films is calculated to be 246, 312, 569, and 725 nm, respectively, and is represented in the inset by the thin films (a)–(d). Additionally, a little reduction in film thickness was seen at cycle 50 (428 nm), which might be related to the development of an outer porous layer and/or stress that tends to promote delamination, which results in the film peeling off after reaching its maximum thickness [20]. After 40 cycles, precipitation commences, and TiO_2 starts to settle on the substrate's surface as a result of a heterogeneous reaction. From Fig. 1, it can be seen that the TiO_2 film's thickness rises with each cycle of deposition. The pictures of TiO_2 thin films formed during various deposition cycles are shown in the inset of Fig. 1.

Study of X-ray diffraction (XRD)

In Fig. 2, the XRD patterns of SILAR-deposited TiO_2 thin films between 10 and 40 deposition cycles, denoted by letters a to d, were displayed. At 723 K, the TiO_2 samples were annealed. The anatase (JCPDS: 00-021-1272) crystal structure of the TiO_2 material is shown by the four strong peaks in the XRD pattern of sample (d) at $2\theta = 24.87, 37.87, 47.66,$ and 62.72 , which correspond to the diffraction planes of (101), (112), (204), respectively. Diffraction peaks became sharper and more intense as deposition cycles progressed. This indicates that increasing the number of dipping cycles enhances the crystallinity of films. The expansion of the peak points to the creation of larger nanocrystals, and the significant peaks in each spectrum attest to the crystalline structure and asymmetric crystal orientation of the produced particles.

Small intensity peaks are visible in the XRD patterns created with 10 SILAR cycles, as shown in Fig. 2(a). All peaks sharpen after 20 deposition cycles (see Fig. 2 (b)). Peaks at 24.87, 37.87, 47.66, and 62.72 at 30 deposition cycles, which correspond to the diffraction planes (101), (112), (200), and (204), respectively, showed the creation of an anatase crystal structure of TiO₂ material (See Fig. 2 (c)). All peaks sharpen when the number of dipping cycles is increased to 40 (see Fig. 2(d)). There are no other peaks visible in the diffraction pattern other than the TiO₂ XRD peaks. As the number of times the films are deposited grows due to their thickness, so does the intensity of the prominent peaks. The well-known Scherer formula is used to estimate the grain size of the samples:

$$D = \frac{0.9 \lambda}{\beta \cos \theta} \quad (6)$$

Where the wavelength of the K_α-X-ray is $\lambda = 1.54$ and β is the full width at half maximum. The sample (101) plane's measured crystalline sizes for the 10, 20, 30, and 40 deposition cycles were 31.32, 32.94, 35.25, and 38.17 nm, respectively.

Fourier-transform infrared spectroscopy

Fourier-transform infrared spectroscopy (FTIR) has been used to conduct infrared spectroscopy on prepared samples. Fig. 3 displays the FTIR spectra of TiO₂ samples created using various deposition cycles. It is noted that a thin band at 534.18 cm⁻¹ appears that can be attributed to the Ti-O bond and is linked to the typical vibrational mode of anatase TiO₂. The TiO₂ bonds found in the deposited films match to the vibrations reflected in the 400–900 cm⁻¹ range [21]. The stretching and bending vibration of the hydroxyl groups in molecular water may be the cause of the absorption peaks at near about 1384 and 1631 cm⁻¹ (H-O-H). The presence of the hydroxide group (O-H), which cannot be avoided in the SILAR method, is shown by the absorption at 3434.6 cm⁻¹. As the number of times the films are deposited grows due to their thickness, so does the intensity of the prominent peaks. The XRD result supports the TiO₂ characteristic peaks in the FTIR analysis, confirming the existence of TiO₂ nanoparticles.

Scanning electron microscopy:

SEM is one of the most effective and promising methods for studying the topography of the materials. The surface morphology, size, and shape of the particles in the film are all crucial details revealed by SEM study. At a magnification of 20,000X, the SEM images of TiO₂ thin films at various deposition cycles are displayed in Fig. 4 (a-d). TiO₂ thin films' surface shape significantly varies during SILAR technique deposition cycles. With each cycle of deposition, the film's particle growth accelerated. The micrograph of the TiO₂ film produced by the SILAR method's 10 deposition cycles is shown in Fig. 4(a). It exhibits the uneven proliferation of particles over the substrate's surface by displaying the uneven division of agglomerated NPs. It doesn't show significant grain development. Fig. 4(b), which depicts the micrograph of a TiO₂ film deposited at 20 deposition cycles, exhibits homogenous and uniform NPs. This was caused by either a decrease in agglomerated particles, which promotes the growth of film surfaces, or by changes in elemental composition ratios following an increase in deposition cycles. Different-oriented discrete NPs are shown in the micrograph. The micrographs of TiO₂ films applied using the SILAR approach at 30 and 40 deposition cycles are shown in Figures 4(c) and (d), respectively. The morphology of the film shows the obvious alteration. In the well-defined boundaries with spherical surface morphology, the figure depicts the non-uniform distribution of aggregated particles. By increasing the deposition cycles, an increase in layer thickness is seen. The adequate bulk formation at room temperature is to the reason for increased film thicknesses.

Optical absorption study:

The UV-Visible spectroscopy was used to gather the information on optical absorption. The samples have high absorption coefficient values of roughly 10⁴ cm⁻¹, it is discovered (see Fig. 5). The following equation relates the incident photon energy ($h\nu$) with the absorption coefficient (α).

$$(\alpha h\nu)^{\frac{1}{n}} = A(h\nu - E_g) \quad (7)$$

Where A is a constant, h is the energy of the incident photon, and n is an exponent that depends on whether the transition is direct or indirect, with n = 1/2 or 2, respectively. The straight part of the energy axis, $(\alpha h\nu)^{\frac{1}{n}} = 0$, might be extrapolated to determine the direct and indirect band gaps. The optical absorption of TiO₂ thin films for various deposition cycles is examined. These spectra showed in Fig. 5 (A), demonstrate the high visible light absorption of TiO₂ thin films, demonstrating the material's suitability as an absorbent substance. From 300 nm to 800 nm, TiO₂ nanoparticles showed high light absorption over a large range. By increasing the SILAR deposition cycles, the TiO₂ nanoparticles' ability to absorb visible light was monotonically improved.

Fig. 5(B) displays the plots of $(\alpha h\nu)^{\frac{1}{n}}$ versus $h\nu$ for all of the TiO₂ samples for various deposition cycles. Plot characteristics point to a direct interband transfer. The band gap energy of the material can be

estimated from the value measured on the x-axis. The optical band gap spectra for thin films with 10, 20, 30, and 40 deposition cycles are depicted in Fig. 5(B) and are denoted by (a), (b), (c), and (d), respectively. For thin films that underwent 10, 20, 30, and 40 deposition cycles, the band gap values were determined to be 3.70, 3.67, 3.65, and 3.59 eV, respectively. As the film thickness increases, the band gap steadily reduces from 3.70 to 3.59 eV, as seen in Fig. 5 (B). Small variations in crystallinity and/or composition may be the cause of the band gap's small decrease with deposition cycles. The quantum size effect brought on by the particles' nano size can be responsible for this difference. The optical characteristics of the film can differ significantly for different TiO₂ material thicknesses depending on the particle size and overall thickness of the films, which are in the nano-domain. Similar findings were also reported by Patil et al. [20] during the SILAR method's fabrication of TiO₂ thin films.

Photoluminescence:

Using photoluminescence (PL) spectroscopy, important details regarding the migration and transfer of charge carriers in semiconductors can be studied. These processes begin when photogenerated electrons and holes undergo radiative recombination. At room temperature, the optical PL of anatase TiO₂ was investigated. Fig. 6 displays the PL spectra for TiO₂ layers of varied thicknesses. Here, we noticed peaks between 550 and 610 nm. The oxygen vacancies in TiO₂ and the self-trapped excitons cause the peaks at 576, 580, and 593 nm [15]. With increase in thin film thickness, the anatase band at 593 nm becomes more noticeable. For sample (a), a thin film of TiO₂ subjected to 10 cycles, the peak's PL intensity is 3348 arbitrary units at a wavelength of 593 nm. Following a 20-cycle increase in TiO₂ thin film thickness at sample (b), a peak at 576 nm with a PL intensity of 3850 arbitrary units was observed. Additional increases in the deposition cycle brought it to 30 cycles, with a peak at 580 nm and a PL intensity of 4012 arbitrary units. Deposition cycle simultaneously increased by up to 40 cycles, with the peak being seen at 593 nm with a PL intensity of 4012 arbitrary units. Fig. 6 shows that the PL intensity was higher for samples that had undergone more SILAR cycles. The sample created using 40 SILAR cycles showed a higher PL intensity than the one created using 10 SILAR cycles. The correlation between PL intensity and photo-induced electron-hole pair recombination rate has been shown [22]. We can therefore draw the conclusion that TiO₂ is a substance employed in an optoelectronic device.

Antimicrobial activity:

With streptomycin (indicated by E) as a positive control and distilled water as a negative control, the antimicrobial potential of synthesized TiO₂ nanoparticles was investigated using the agar gel diffusion method to the zone of inhibition of two bacterial strains: *S. aureus* (NCIM-2654) gram-positive, and *P. aeruginosa* (NCIM-5032) gram-negative bacteria. Similar to this, *C. albicans* (NCIM-3466) is one of the fungi that fluconazole (indicated by F) inhibits when used as the standard medication against a suspension of TiO₂ nanoparticles. For the evaluation of bacterial inactivation, solid auger disc diffusion has been identified utilizing all TiO₂ samples generated at various deposition cycles and incubated at 37°C for 24 hours (Fig. 7a) (A-D). Each sample's TiO₂ suspension droplets were applied using round filter paper in a disc. Photograph depicting the antibacterial activity of TiO₂ nanoparticles against two bacterial strains (*S. aureus* and *P. aeruginosa*) and one fungus (*C. albicans*) is shown in Fig. 7a. According to these antibacterial investigations, the well contains TiO₂ nonmaterial, which prevents the growth of *S. aureus*, *P. aeruginosa*, and *C. albicans*. The current investigation verified that TiO₂ effectively combats *P. aeruginosa* and *Candida albicans*. The antimicrobial and antifungal activity on *Staphylococcus aureus*, *Pseudomonas aeruginosa*, and one fungal strain, *Candida albicans*, was observed in Fig. 7a. Sample A-TiO₂ recorded the maximum inhibition, which is significantly higher than samples B-TiO₂, C-TiO₂, and D-TiO₂ samples carried 32.94, 35.25, and 38.17 nm crystallite size, The statistical bar analysis of TiO₂-NPs against the tested microbial and fungal species is shown in Fig. 7b.

For these samples, which were prepared by 10 SILAR cycles, we obtained excellent antibacterial activity (Table 1, Entry I). Table 1, Entry II, III, and IV in the other TiO₂ material do not provide good results. The smaller crystallite size in the 10 SILAR cycle sample is what causes the increased antibacterial activity. From these, it can be seen that 10 SILAR cycles with decreased crystallite size work together synergistically to produce excellent antibacterial action. The antibacterial activity of TiO₂ nanoparticles with smaller crystallite sizes was higher than that of those with larger crystallite sizes. We discovered that the antibacterial activity of TiO₂ NPs is directly influenced by the size of the crystallites. Reactive oxygen species (ROS), which are produced by TiO₂ nanoparticles that have been spread, are mostly linked to oxidative stress and bacterial degradation. Bacteria's cell membrane, which protects it from the harsh environment, is an essential component [23]. Bacterial deactivation begins with membrane damage, which points to physiochemical modification privileged the membrane. Bonds are disrupted when ROS cause stress on a membrane by destroying the PUFA acids and crust lipids that lie beneath the membrane. In the future, aldehydes, a hazardous reactive messenger, destroy inner protein molecules and lead to membrane leakage, which renders bacteria inactive [24]. Additionally, in-depth analysis of the

antibacterial properties of crystalline ceramics has revealed that the activity was influenced by crystallographic elements including the lattice constant [25].

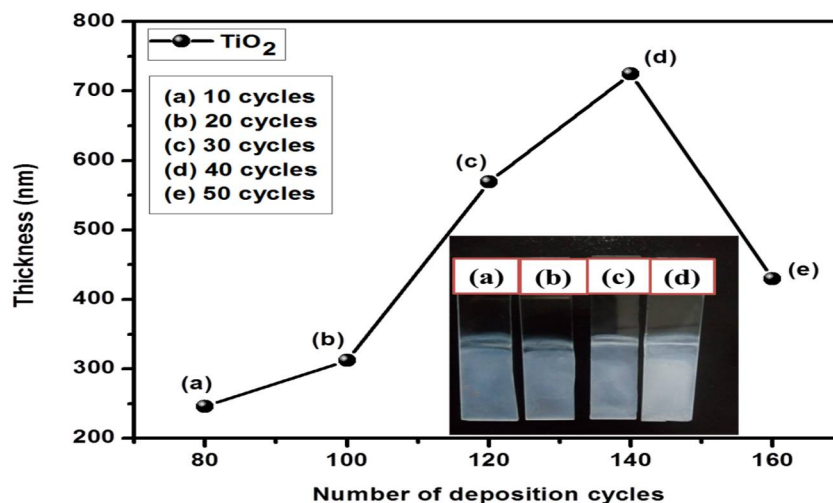


Fig. 1 Variations of TiO₂ film thickness with various deposition cycles. Inset of the figure shows the photograph of TiO₂ thin films deposited at various deposition cycles.

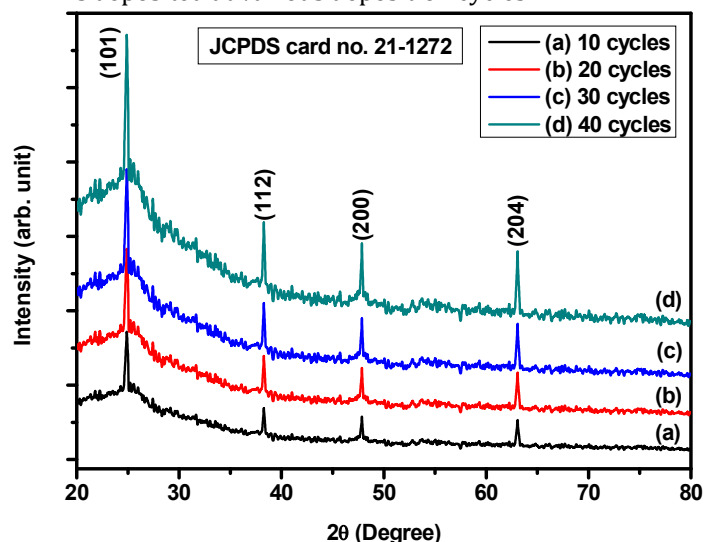


Fig. 2 X-ray diffraction spectra of SILAR deposited TiO₂ thin films at various deposition cycles.

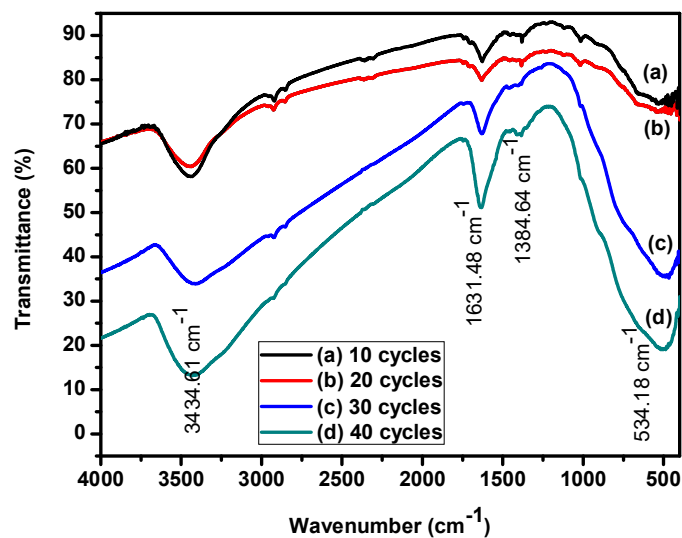


Fig. 3 FTIR spectra of SILAR deposited TiO₂ thin films at various deposition cycles.

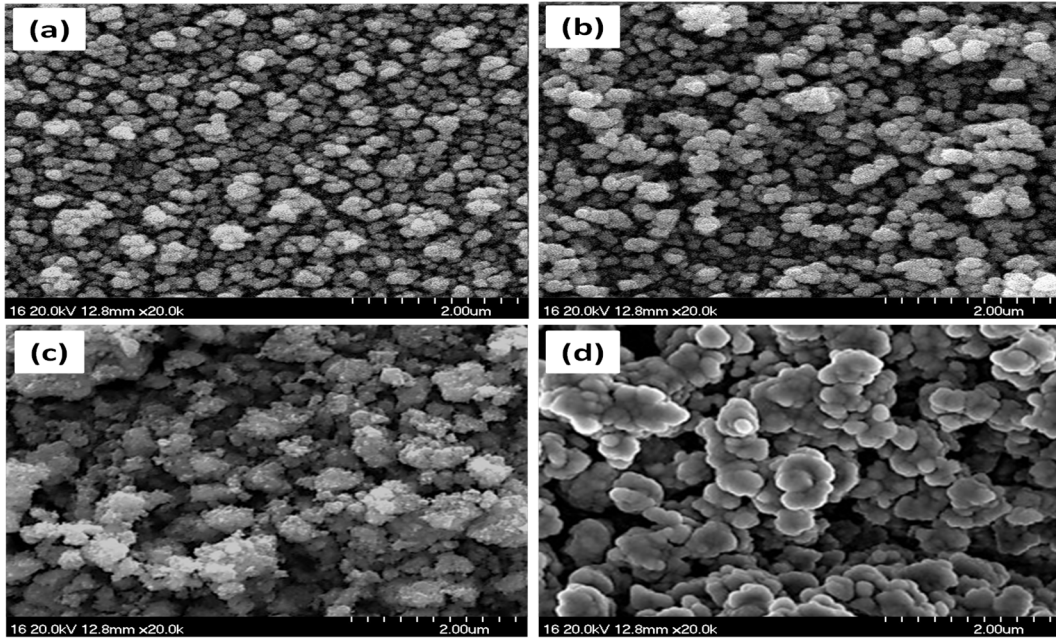


Fig. 4 SEM micrographs of at 15000X magnifications of TiO₂ thin films at various deposition cycles.

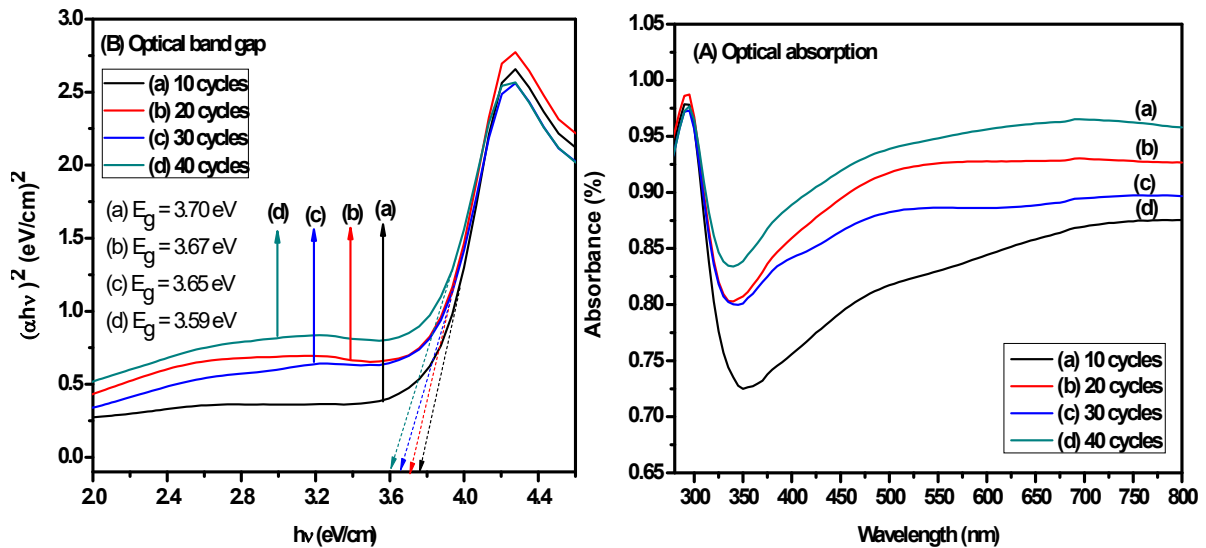


Fig. 5(A) Optical absorption spectra and (B) optical band gap plots of TiO₂ thin films at various deposition cycles.

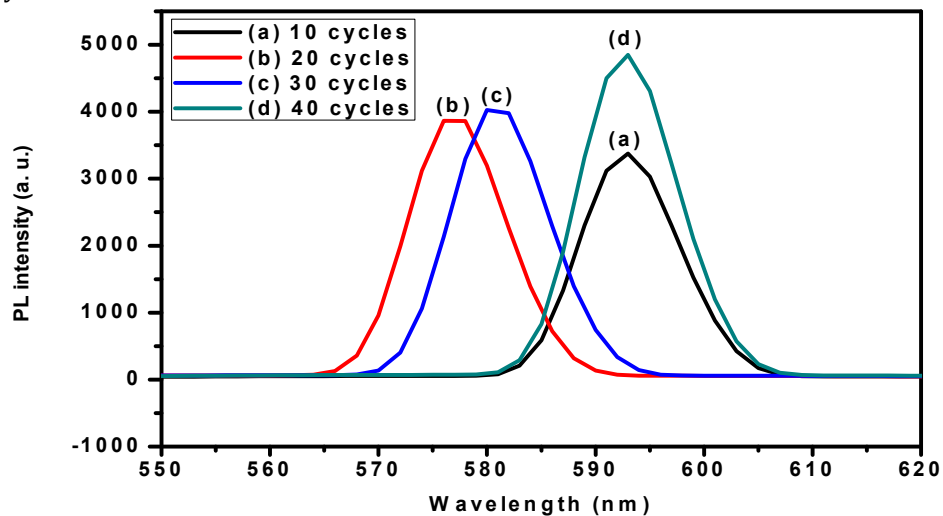


Fig. 6 Photoluminescence spectra of SILAR deposited TiO₂ thin films at various deposition cycles.

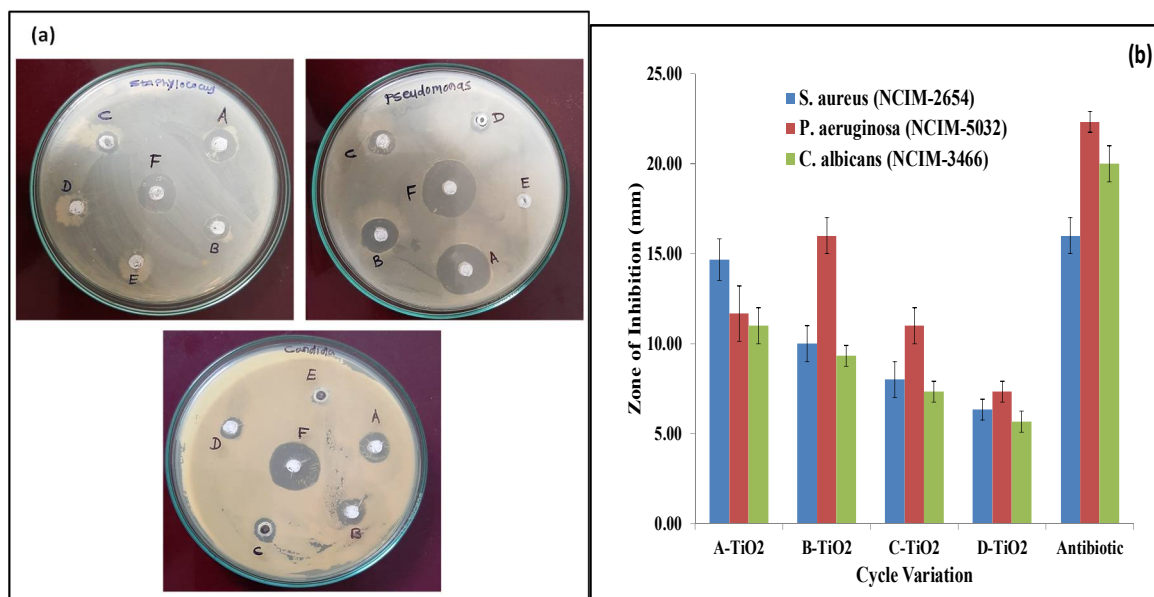


Fig. 7 (a) Antimicrobial and antifungal activity on the *Staphylococcus aureus*(NCIM -2654), *Pseudomonas aeruginosa*(NCIM - 5032) and one fungal strains *Candida albicans*(NCIM - 3466) for TiO₂Zone of inhibition at various thicknesses i.e. A-TiO₂10 SILAR Cycles, B-TiO₂20 SILAR Cycles, C-TiO₂ 30 SILAR Cycles, D-TiO₂40 SILAR Cycles,E - Control and F - Antibiotic and **Fig. 7 (b)** The statistical analysis of TiO₂-NPs against tested microbial and fungal organisms

Table 1 The mean ± standard error of three replicates is *Staphylococcus aureus*(NCIM -2654), *Pseudomonas aeruginosa*(NCIM - 5032) and *Candida albicans*(NCIM - 3466).

Sample	Crystallite size (nm)	Antibacterial activity (mm)		Antifungal activity (mm)
		<i>Staphylococcus aureus</i>	<i>Pseudomonas aeruginosa</i>	<i>Candida albicans</i>
A-TiO ₂	31.32	14.67 ± 1.15	18.67 ± 1.53	11.00 ± 1.00
B-TiO ₂	32.94	10.00 ± 1.00	16.00 ± 1.00	9.33 ± 0.58
C-TiO ₂	35.25	8.00 ± 1.00	11.00 ± 1.00	7.33 ± 0.58
D-TiO ₂	38.17	6.33 ± 0.58	7.33 ± 0.58	5.67 ± 0.58
E-Streptomycin	-	16.00 ± 1.00	22.33 ± 0.58	NA
F-Fluconazole	-	NA	NA	20.00 ± 1.53

CONCLUSION

In conclusion, the simple and cost-effective SILAR approach has been successful in depositing TiO₂ thin films at ambient temperature. TiO₂ thin film's structural, morphological, and optical characteristics are explored in relation to thickness. TiO₂ has nanocrystalline structure with anatase phase, according to XRD investigations. With increased thickness, the films' crystallinity improved. The FTIR analysis supported the discovery of pure phases in the TiO₂ compound. The results of the morphological investigation showed that the films' homogeneous, smooth, and compact nature grew stronger as their thickness increased. Additionally, the optical band gap shrank as thickness increased, which is connected to variations in crystal composition and/or crystallinity. Using *S. aureus*, *P. aeruginosa*, and *C. albicans*, the antibacterial activity of the TiO₂ samples utilized in this investigation was assessed using the Agar well diffusion method. We discovered that the synergistic effect of the number of cycles with the size of TiO₂ particles plays a vital role in the good antibacterial activity. Regardless of the type of sample, we found that samples with small crystallite sizes exhibited higher antibacterial activity than samples with large crystallite sizes. These findings showed that crystallite size affects the antibacterial activity of TiO₂ samples.

ACKNOWLEDGEMENT:

The author is grateful to the Mahatma JyotibaPhule Research Fellowship (MJPRF-2021) for funding. Authors also like to acknowledge Department of Physics, Yashwantrao Chavan Institute of Science, Satara, Maharashtra, India for providing kind support during this study.

REFERENCES

1. M. Hajipour, K. Fromm, A. Akbar, A. Jimenez, I. Larramendi, T. Rojo, Trends Biotechnol., 30 (2012) 499-511.
2. G. Whitesides, Small, 1 (2005) 172-179.
3. T. Puzyn, B. Rasulev, A. Gajewicz, X. Hu, T. Dasari, A. Michalkova, Nature Nanotechnology, 6 (2011) 175-178.
4. X. He, P. Fu, W. Aker, H. Hwang, Journal of Environmental Science and Health - Part C Environmental Carcinogenesis and Ecotoxicology Reviews, 36 (2018) 21-42.
5. H. Hwang, P. Ray, H. Yu, X. He, In book: Sustainable preparation of metal nanoparticles {Chapter 8} (2012) 190-212.
6. M. Shah, D. Fawcett, S. Sharma, S. Tripathy, G. Poinern, Materials., 8 (2015) 7278-7308.
7. S. Subhapriya, P. Gomathipriya, Microbial Pathogenesis, 116 (2018) 215-220.
8. Y. Leung, X. Xu, A. Ma, F. Liu, A. Ng, Z. Shen, L. Gethings, M. Guo, A. Djuriši, P. Lee, Sci. Rep., 6 (2016) 35243.
9. N. Kashef, Y. Huang, R. Hamblin, Nanophotonics, 6 (2017) 853.
10. M. Brushan, Y. Kumar, L. Periyasamy, A. Viswanath, Appl. Nanosci., 8 (2018) 137.
11. A. Abbaszadegan, Y. Ghahramani, A. Gholami, B. Hemmateenejad, S. Dorostkar, M. Nabavizadeh, H. Sharghi, J. Nanomater., 2015 (2015) 720654.
12. L. Gabrielyan, A. Hovhannisy, V. Gevorgyan, M. Ananyan, A. Trchounian, Appl. Microbiol. Biotechnol., 103 (2019) 2773.
13. C. Bankier, R. Matharu, Y. Cheong, G. Ren, E. Cloutman, L. Ciric, Sc. Rep., 9 (2019) 16074.
14. S. Vihodcev, A. Šutka, M. Sihtmäe, M. Rosenberg, M. Otsus, I. Kurvet, K. Smits, L. Bikse, A. Kahru, K. Kasemets, Nanomaterials, 11 (2021) 652.
15. S. Khan, M. Al-Shahry, W. Ingler, Science, 297 (2002) 2243-2245.
16. I. Chung, I. Park, K. Seung-Hyun, M. Thiruvengadam, G. Rajakumar, Nanoscale Research Letters, 11 (2016) 1-14.
17. A. Bui, A. Bacic, F. Pettolino, Phytochemistry, 67 (2006) 1271-1275.
18. P. Ravikumar, S. Kumar, International Journal of Technical Research and Applications. 2 (2014) 108-111.
19. L. Inbathamizh, T. Ponnu, E. Mary, Journal of Pharmacy Research, 6 (2013) 32-38.
20. U. Patil, K. Gurava, O. Joo, C. Lokhande, Journal of Alloys and Compounds 478 (2009) 711-715.
21. C. Brundha, C. Karthikeyan and S. Karuppuchamy, Journal of Physical Sciences, 1 (2017) 76-81.
22. Z. Xie, X. Liu, W. Wang, C. Liu, Z. Li, Z. Zhang, Sci. Technol. Adv. Mater., 15 (2014) 055006-055012.
23. M. Zaman, R. Poolla, P. Singh, T. Gudipati, Environ. Nanotechnol. Monit. Manag., 14 (2020) 100346 (1-10).
24. A. Ali, S. Ahmed, J. Rehman, M. Abdullah, H. Chen, B. Guo, Y. Yang, Mater. Today Commun., 26 (2021) 101675 (1-9).
25. T. Ohira and O. Yamamoto, Chem. Eng. Sci., 68 (2012) 355-361.

CITATION OF THIS ARTICLE

A. A. Mohite, A. A. Survase, M. M. Faras, H. D. Shelke, A. D. Kadam, A. S. Jadhav, and A. P. Torane: Influence of particle size on antibacterial and antifungal strains of titanium dioxide (TiO₂) nanoparticles synthesized by SILAR method. Bull. Env. Pharmacol. Life Sci., Spl Issue [1]: 2023:256-264.